Journal of Hazardous Materials 197 (2011) 320–326

Contents lists available at SciVerse ScienceDirect

Journal of Hazardous Materials

journal homepage: www.elsevier.com/locate/jhazmat

Synthesis of Au nanoparticles decorated graphene oxide nanosheets: Noncovalent functionalization by TWEEN 20 in situ reduction of aqueous chloroaurate ions for hydrazine detection and catalytic reduction of 4-nitrophenol

Wenbo Lu[a], Rui Ning[a,b], Xiaoyun Qin[a], Yingwei Zhang[a], Guohui Chang[a], Sen Liu[a], Yonglan Luo[a], Xuping Sun[a,*]

[a] State Key Laboratory of Electroanalytical Chemistry, Changchun Institute of Applied Chemistry, Chinese Academy of Sciences, Changchun 130022, Jilin, China
[b] Graduate School of the Chinese Academy of Sciences, Beijing 100039, China

ARTICLE INFO

Article history:
Received 15 August 2011
Received in revised form
23 September 2011
Accepted 23 September 2011
Available online 1 October 2011

Keywords:
TWEEN 20
Graphene oxide
Au nanoparticle
4-Nitrophenol
Hydrazine detection

ABSTRACT

In this paper, we develop a cost-effective and simple route for the synthesis of Au nanoparticles (AuNPs) decorated graphene oxide (GO) nanosheets using polyoxyethylene sorbitol anhydride monolaurate (TWEEN 20) as a stabilizing agent for GO as well as a reducing and immobilizing agent for AuNPs. The AuNPs assemble on the surface of TWEEN-functionalized GO by the in situ reduction of $HAuCl_4$ aqueous solution. The morphologies of these composites were characterized by atomic force microscopy (AFM) and transmission electron microscopy (TEM). It is found that the resultant AuNPs decorated GO nanosheets (AuNPs/TWEEN/GO) exhibit remarkable catalytic performance for hydrazine oxidation. This hydrazine sensor has a fast amperometric response time of less than 3 s. The linear range is estimated to be from 5 μM to 3 mM (r = 0.999), and the detection limit is estimated to be 78 nM at a signal-to-noise ratio of 3. The AuNPs/TWEEN/GO composites also exhibit good catalytic activity toward 4-nitrophenol (4-NP) reduction and the GO supports also enhance the catalytic activity via a synergistic effect.

1. Introduction

Graphene, a free-standing two-dimensional crystal with a single layer structure, has become one of the hottest of topics in the fields of physics, chemistry, nanotechnology and materials science [1–4]. Graphene-based nanocomposites have stimulated intense research over past decades because of their new optical, electronic, mechanical, and catalytic properties [4–7]. Particularly, due to the large surface area and above mentioned properties, graphene oxide (GO) has been an attractive choice as the substrate for nanocomposites [8–11]. Among them, Au nanoparticles (AuNPs)/GO nanocomposites have attracted immense attention [12,13]. It is well-documented that AuNPs play a key role in electrocatalytic reactions and AuNPs modified electrodes exhibit higher electrocatalytic activities for the detection of some small molecules such as hydrazine [14], H_2O_2 [15], and nitric oxide [16] than other traditional modified electrodes. Meanwhile, AuNPs also show a good catalytic activity for reduction of 4-nitrophenol (4-NP) [17]. More recently, many efforts have been devoted to the design of AuNPs supported on GO sheets. For example, Pham and coworkers have reported a method for immobilization of AuNPs on GO sheets by covalent bonding [18]. Zhou et al. have prepared AuNPs/GO composites obtained by immersing the Ag nanoparticles/GO composites in the $HAuCl_4$ solution [9]. However, all the above-mentioned methods suffer from more or less drawbacks, such as the prior GO functionalization [18] and the multiple-step preparation process [9]. Accordingly, the development of new preparation strategy overcoming all the shortcomings is highly desired.

Hydrazine is extensively used in chemistry industry, aerospace industry and pharmaceutical field, including catalysts, fuel cell, rocket fuels, high-energy propellant, missile systems, herbicide and pesticide [19–23]. It is a neurotoxin, and hence produces mutagenic and carcinogenic effects causing damage to kidneys, lungs, liver, respiratory tract infection and long-term effects on the central nervous system [20,21]. Due to the above reasons, it is highly desirable to fabricate a sensitive analytical tool for the effective detection of hydrazine. Water pollution by phenol and phenolic compounds is of tremendous public concern. Nitrophenols and their derivatives, which result from the production processes of pesticides, insecticides, synthetic dyes and herbicides, are some of the most refractory pollutants that occur in industrial wastewaters [24–26]. The United

* Corresponding author. Tel.: +86 431 85262065; fax: +86 431 85262065.
E-mail address: sunxp@ciac.jl.cn (X. Sun).

0304-3894/$ – see front matter © 2011 Elsevier B.V. All rights reserved.
doi:10.1016/j.jhazmat.2011.09.092

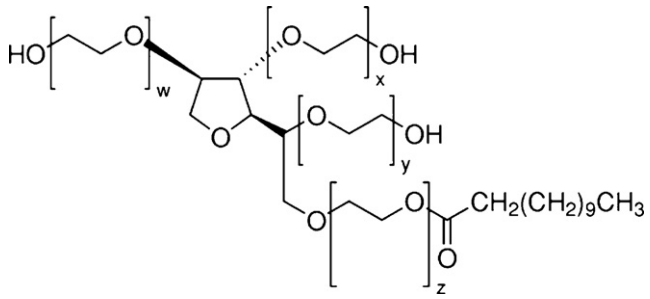

Fig. 1. The chemical structure of TWEEN 20.

States Environmental Protection Agency lists nitrophenols among the top 114 organic pollutants [25]. Because of the aforesaid reasons, this study for catalytic reduction of 4-nitrophenol becomes more fascinating from the point of pollution abatement.

Polyoxyethylene sorbitol anhydride monolaurate (TWEEN 20), a commercially available and innoxious chemical with aliphatic ester chains, is composed of three chemical sections (as shown in Fig. 1): aliphatic ester chains that can prevent nonspecific binding of biomolecules, an aliphatic chain that can easily be adsorbed on a hydrophobic surface by noncovalent interaction, and three-terminal hydroxyl groups that are hydrophilic and can be chemically modified for further applications. Although Park et al. have fabricated a strong TWEEN 20 dispersion of chemically reduced GO composites [27], the synthesis and applications of nanoparticle-decorated TWEEN/GO composites have not been reported. In this paper, we report on our recent finding that AuNPs can be in situ reduced and immobilized on TWEEN 20-functionalized GO through a cost-effective strategy with the use of TWEEN 20 as a stabilizing agent for GO [27] as well as a reducing and immobilizing agent for Au nanoparticles. Scheme 1 illustrates the noncovalent functionalization of GO by TWEEN 20 and the subsequent in situ synthesis of AuNPs on TWEEN/GO. It was found that the resultant AuNPs decorated TWEEN/GO (AuNPs/TWEEN/GO) composites exhibit notable catalytic performance toward hydrazine oxidation. Meanwhile, the AuNPs/TWEEN/GO composites exhibit good activity in catalyzing the reduction of 4-nitrophenol (4-NP) by $NaBH_4$ and the GO support has a synergistic effect to enhance the catalytic activity of AuNP catalysts.

2. Experimental

2.1. Materials

TWEEN 20, $HAuCl_4$, NaH_2PO_4, Na_2HPO_4, graphite, chitosan and H_2O_2 (30 wt%) were purchased from Aladin Ltd. (Shanghai, China). $KMnO_4$, $NaNO_3$, ammonium hydroxide ($NH_3{\cdot}H_2O$) (28 wt% in water), H_2SO_4, ethanol were purchased from Shanghai Chemical Factory (Shanghai, China). All chemicals were used as received without further purification. The water used throughout all experiments was purified through a Millipore system. Phosphate buffer saline (PBS) was prepared by mixing stock solutions of NaH_2PO_4 and Na_2HPO_4 and a fresh solution of H_2O_2 was prepared daily.

2.2. Instruments

Atomic force microscopy (AFM) was conducted with a SPI3800N microscope (Seiko Instruments, Inc.). UV–vis spectra were collected on a UV5800 modal spectrophotometer. Transmission electron microscopy (TEM) measurements were made on a HITACHI H-8100 EM (Hitachi, Tokyo, Japan) with an accelerating applied potential of 200 kV. The sample for TEM characterization was prepared by placing a drop of the dispersion on carbon-coated copper grid and dried at room temperature. Electrochemical measurements are performed with a CHI 660D electrochemical analyzer (CH Instruments, Inc., Shanghai). A conventional three-electrode cell is used, including a GCE (geometric area = 0.07 cm^2) as the working electrode, a Ag/AgCl (3 M KCl) electrode as the reference electrode, and platinum foil as the counter electrode. All potentials given in this work are referred to the Ag/AgCl electrode. All the experiments are carried out at ambient temperature.

2.3. Preparation of GO

GO was prepared from natural graphite powder through a modified Hummers method [28]. In a typical synthesis, 1 g of graphite was added into 23 mL of 98% H_2SO_4, followed by stirring at room temperature over a 24 h period. After that, 100 mg of $NaNO_3$ was introduced into the mixture and stirred for 30 min. Subsequently, the mixture was kept below 5 °C by ice bath, and 3 g of $KMnO_4$ was slowly added into the mixture. After being heated to 35–40 °C, the mixture was stirred for another 30 min. After that, 46 mL of water was added into above mixture during a period of 25 min. Finally, 140 mL of water and 10 mL of 30% H_2O_2 were added into the mixture to stop the reaction. After the unexploited graphite in the resulting mixture was removed by centrifugation, as-synthesized GO was dispersed into individual sheets in distilled water at a concentration of 0.5 mg/mL with the aid of ultrasound for further use.

2.4. Synthesis of AuNPs/TWEEN/GO composites

In a typical synthesis, 400 μL of TWEEN 20 (0.4 g/mL) solution was added into 1 mL of GO (0.6 mg/mL) aqueous solution, and then the mixture was sonicated for 30 min. Next, the mixture was centrifuged and the precipitates were redispersed in 0.5 mL of water. After that, 40 μL of 24.3 mM $HAuCl_4$ and 12 μL of 1 M NaOH aqueous solution were added into the previous solution under relatively mild shaking. The color of the resulting solution changed to dark-red after 5 s at room temperature.

2.5. Synthesis of TWEEN 20 stabilized AuNPs

As a control experiment, TWEEN 20 stabilized AuNPs (AuNPs/TWEEN) were also synthesized in the same way as synthesis of AuNPs/TWEEN/GO composites by mixing 40 μL of $HAuCl_4$ aqueous solution (24.3 mM) and 100 μL of TWEEN 20 (0.4 g/mL), and then 12 μL of 1 M NaOH aqueous solution was added into the mixture under relatively mild shaking. The color of the solution changed to dark-red after 3 s at ambient temperature. Finally, the mixture was diluted to 552 μL with water.

2.6. Electrocatalytic and optical experiments

The modified electrodes were prepared by a simple casting method. Prior to the surface coating, the GCE was polished with 1.0 and 0.3 μm alumina powder, respectively, and rinsed with doubly distilled water, followed by sonication in ethanol solution and doubly distilled water successively. Then, the electrode was allowed to dry in a stream of nitrogen. For the cyclic voltammetry experiment, 100 μL of AuNPs/TWEEN/GO composites was dropped on the surface of pretreated GCE and left to dry at room temperature. For current time experiment, 2 μL of chitosan (0.3%) was additionally cast on the surface of the above modified GCE and dried before electrochemical experiments. For the catalytic reduction of 4-nitrophenol (4-NP), freshly prepared aqueous solution of $NaBH_4$ (1.0 mL, 0.16 M) was mixed with 4-NP aqueous solution (1.0 mL, 7 mM) in the quartz cell (1.5 cm path length), leading a color change from light yellow to yellow-green. Then, the catalysts were added

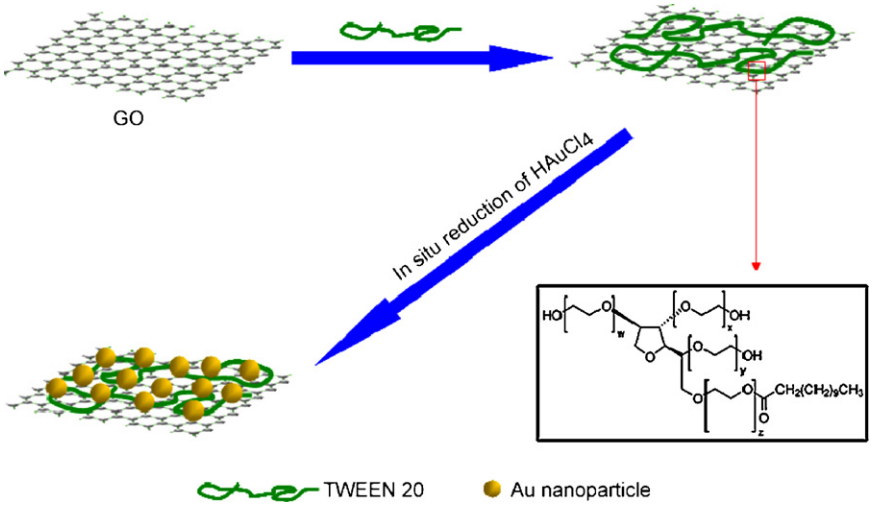

Scheme 1. A scheme (not to scale) to illustrate the noncovalently functionalization of GO by TWEEN 20 and the subsequent preparation of AuNPs/TWEEN/GO composites by in situ chemical reduction of gold salts.

into the mixture and immediately placed in the cell holder of the spectrophotometer. UV–vis absorption spectroscopy was used to monitor the progress of the conversion of 4-NP to 4-aminophenol (4-AP) in the presence of AuNPs/TWEEN/GO catalysts (containing Au: 2.16 mM) by recording the time-dependent adsorption spectra of the reaction mixture in a scanning range of 200–600 nm at ambient temperature.

3. Results and discussion

Fig. 2 shows the UV–vis absorption spectra of GO and AuNPs/TWEEN/GO dispersion. It is obviously seen that the GO dispersion exhibits two characteristic peaks, a maximum at 231 nm, which corresponds to $\pi \rightarrow \pi^*$ transitions of aromatic C–C bonds, and a shoulder at 300 nm, which is attributed to $n \rightarrow \pi^*$ transitions of C=O bonds (curve a) [29]. The two characteristic peaks are also observed in the AuNPs/TWEEN/GO dispersion (curve b). The shoulder peak at 300 nm has become weak due to the interaction between TWEEN 20 and GO. A peak at 521 nm is also observed (curve b), which is attributed to the formation of the AuNPs [30]. The inset in Fig. 2 shows the photographs of the supernatant

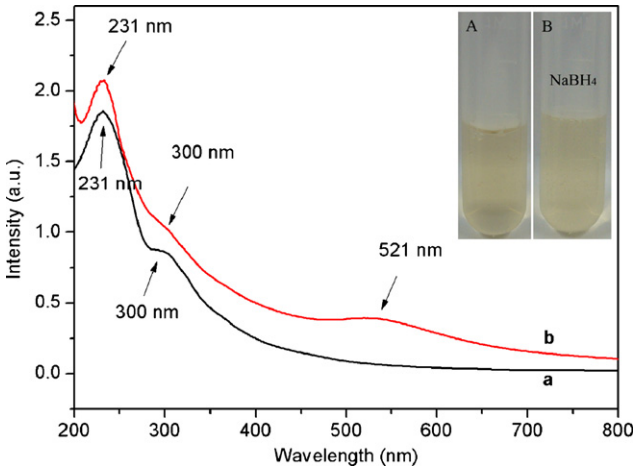

Fig. 2. UV–vis absorption spectra of aqueous dispersions of (a) GO and (b) AuNPs/TWEEN/GO. Inset: photographs of the supernatant of the AuNPs/TWEEN/GO dispersion acquired by centrifugation (A) before and (B) after adding $NaBH_4$ aqueous solution.

of the AuNPs/TWEEN/GO dispersion acquired by centrifugation before and after adding 0.3 mL of 1 M $NaBH_4$ aqueous solution. The observation of no color change indicates that all $HAuCl_4$ precursors have been completely reduced. As a result, the mass ratio of GO to $HAuCl_4$ is about 2:1 (theoretical value according to Section 2). The corresponding energy-dispersive spectrum (EDS) of the AuNPs/TWEEN/GO composites is shown in Fig. 3. Two peaks of C and O elements are observed, indicating they are products formed from GO and TWEEN 20. The peak of Au element is also observed, indicating the loading AuNPs on GO (other peaks originated from the glass substrate used). All these observations indicate the AuNPs/TWEEN/GO composites are formed.

To get further information on the AuNPs/TWEEN/GO composites thus obtained, we examined the composites by AFM and TEM analyses. Fig. 4A shows the AFM image of GO sheets. It is obviously seen that the GO sheet range from about 1.5 μm to 3 μm in width. A large amount of GO nanosheets are shown in Fig. 4A, indicating the successful preparation of GO by Hummers method [28]. The GO sheets are measured to be range from approximately 1 μm to 4 μm in lateral dimensions. Fig. 4B and C shows the TEM images of TWEEN/GO and AuNPs/TWEEN/GO composites, respectively, revealing the formation of AuNPs (black dots) on the surface of TWEEN/GO after in situ reduction of $HAuCl_4$. A high magnification TEM image of the AuNPs/TWEEN/GO composites shown in Fig. 4D further reveals that the AuNPs are spherical in shape and

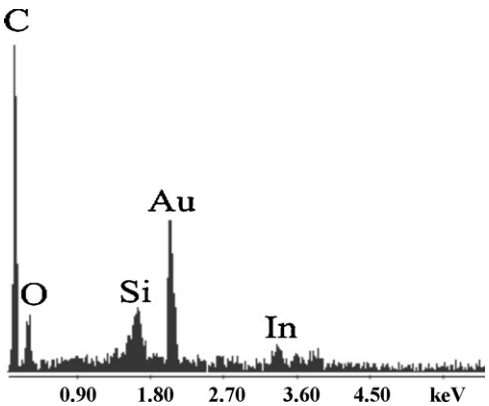

Fig. 3. The corresponding energy-dispersive spectrum (EDS) of the AuNPs/TWEEN/GO composites.

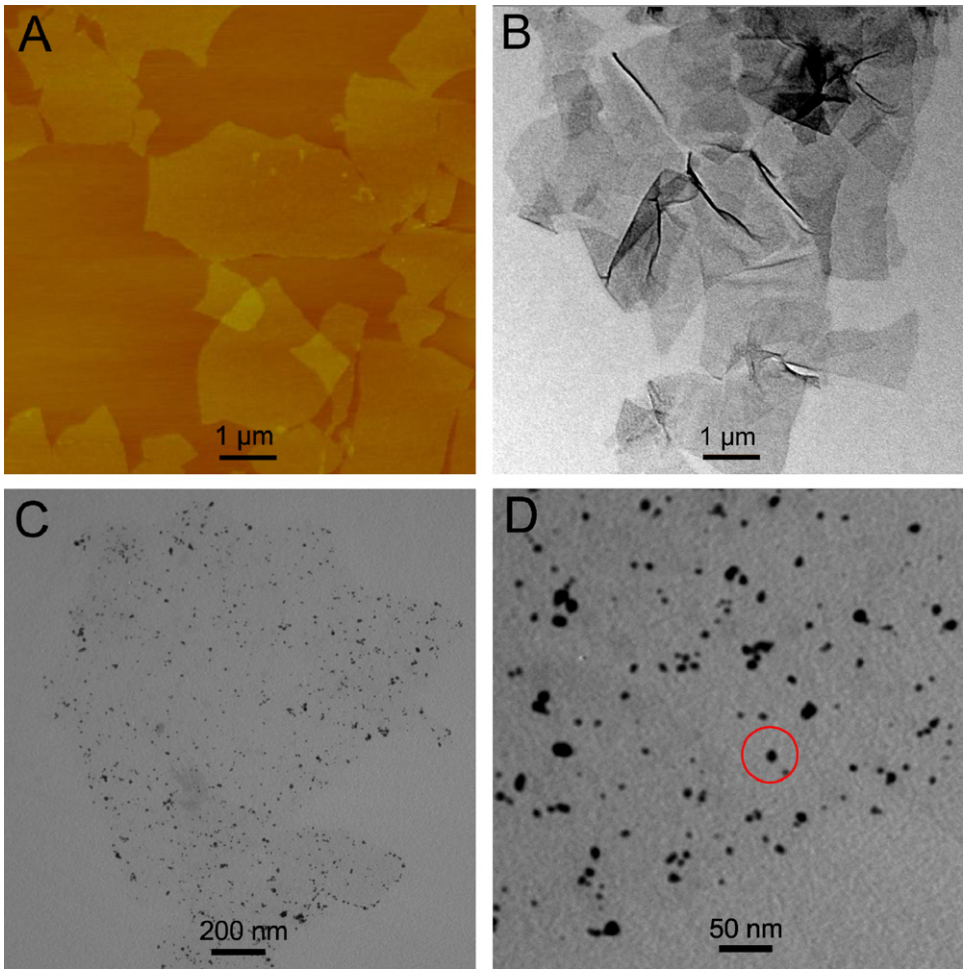

Fig. 4. (A) AFM image of GO nanosheets, TEM images of (B) TWEEN/GO and (C and D) AuNPs/TWEEN/GO composites.

have diameters ranging from 6 nm to 15 nm. All these observations indicate that AuNPs/TWEEN/GO composites are formed. The GO sheets have hydroxyl and epoxy functional groups located at the nanosheets edges [31] and such functional groups have been used as anchors for adsorption of polar materials and inorganic nanoparticles [32]. Both these hydroxyl and epoxy functional groups of GO and hydroxyl groups of TWEEN are believed to be responsible for the effective adsorption of AuNPs on TWEEN/GO in our present study. When sodium hydroxide is added, $[AuCl_4]^-$ reacts with OH^- to $[Au(OH)_nCl_{4-n}]^-$ which can be reduced much easier by TWEEN 20 [33,34]. The reduction of these ions by the TWEEN 20 allows these AuNPs formed by the in situ reduction process to attach onto TWEEN/GO.

We designed a hydrazine sensor by immobilizing AuNPs/TWEEN/GO composites on the GCE. It is found that the resultant AuNPs/TWEEN/GO composites exhibit good catalytic performance toward hydrazine oxidation. Fig. 5 shows the electrocatalytic responses of bare GCE, GO modified GCE (GO/GCE), AuNPs/TWEEN/GO modified GCE (AuNPs/TWEEN/GO/GCE) and AuNPs/TWEEN decorated GCE (AuNPs/TWEEN/GCE) toward the oxidation of hydrazine in 0.2 M PBS at pH 7.4 in the presence of 10 mM hydrazine. We also performed one control experiment by studying the CV behavior of AuNPs/TWEEN/GO/GCE in the absence of hydrazine. In the presence of 10 mM hydrazine, the AuNPs/TWEEN/GO/GCE exhibits a notable current peak about 324.5 μA in intensity centered at 0.45 V vs. Ag/AgCl is observed (line d in Fig. 5); however, it exhibits no electrochemical response in the absence of hydrazine (line b in Fig. 5). These observations indicate that the observed current peak originates from hydrazine oxidation. In contrast, the response of the bare GCE and GO/GCE toward the oxidation of hydrazine is quite weak and even can be neglected (line a and c in Fig. 5). These observations show that the AuNPs contained in the GO composites exhibit an excellent

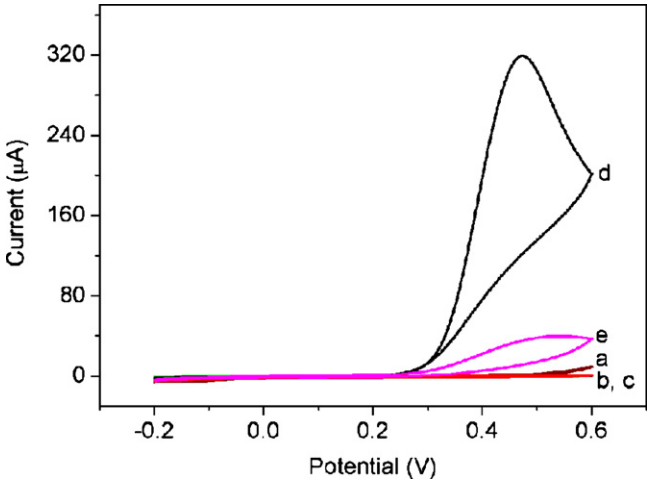

Fig. 5. Cyclic voltammograms (CVs) of (a) bare GCE, (c) GO/GCE, (d) AuNPs/TWEEN/GO/GCE and (e) AuNPs/TWEEN/GCE in 0.2 M PBS at pH 7.4 in the presence of 10 mM hydrazine. (b) CV of AuNPs/TWEEN/GO/GCE in the absence of hydrazine (scan rate: 0.1 V/s).

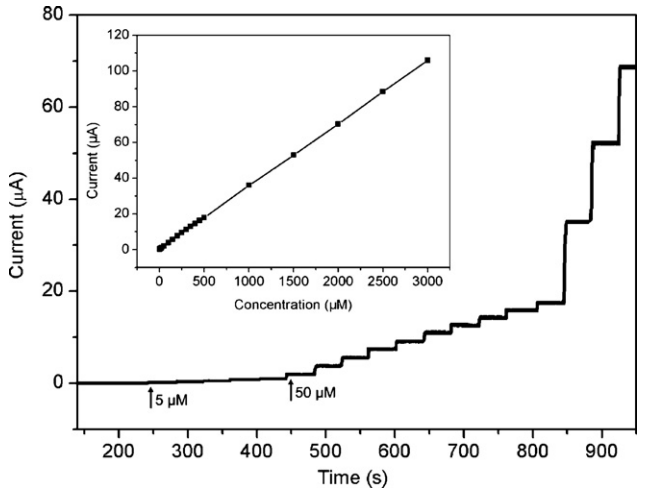

Fig. 6. Typical steady-state response of the AuNPs/TWEEN/GO/GCE to successive injection of hydrazine into the stirred 0.2 M PBS at pH 7.4 (applied potential: 0.40 V). Inset: the fitting of the experimental data by the regression line.

catalytic performance for hydrazine oxidation, and the large catalytic current obtained could be attributed to the loading of the large numbers of AuNPs contained in the GO composites on the surface of GCE. Meanwhile, the AuNPs/TWEEN/GCE exhibits a notable current peak about 39.5 μA in intensity centered at 0.57 V vs. Ag/AgCl (line e in Fig. 5). Compared to the AuNPs/TWEEN/GCE, the T-AuNP/GO/GCE exhibits a better catalytic performance due to the larger effective contact area of AuNPs/TWEEN/GO composites. All the above observations indicate that the AuNPs/TWEEN/GO composites exhibit remarkable electrocatalytic response toward the oxidation of hydrazine. The AuNPs/TWEEN/GO/GCE also shows a good stability. When the AuNPs/TWEEN/GO/GCE was stored at 4 °C in refrigerator for about 15 days, it still retained about 93.5% of its initial sensitivity to the oxidation of hydrazine. Meanwhile, the reproducibility of the AuNPs/TWEEN/GO/GCE was estimated at a PBS buffer solution containing hydrazine concentration of 10 mM with the same decorated electrode. The relative standard deviation (RSD) was 3.9% for 6 successive measurements, indicating the good reproducibility of the AuNPs/TWEEN/GO/GCE.

The AuNPs/TWEEN/GO/GCE also shows good amperometric responses for the electrocatalytic oxidation of hydrazine. Fig. 6 shows typical current–time plot of the AuNPs/TWEEN/GO/GCE in 0.2 M PBS buffer (pH 7.4) on consecutive step change of hydrazine concentrations. When an aliquot of hydrazine was dropped into the stirring PBS solution, the reduction current rose steeply to reach a stable value. The sensor could accomplish 97% of the steady state current within 3 s, indicating a fast amperometric response behavior. It is apparently seen that the steps showed in Fig. 5 are more horizontal in the region of lower concentration of hydrazine and the noises become higher with increased concentration of hydrazine. The inset in Fig. 6 shows the calibration curve of the sensor. The linear detection range is estimated to be from 5 μM to 3 mM (r = 0.999), and the detection limit is estimated to be 78 nM at a signal-to-noise ratio of 3. Compared to the immobilization of AuNPs on the thiolated single-straded DNA decorated Au electrode [35], the detection limit of hydrazine sensor designed herein is much lower. The detection limit of the AuNPs/TWEEN/GO modified hydrazine sensor is also lower than the previously reported amperometric hydrazine sensor based on ZnO modified electrode [36].

4-Aminophenol (4-AP) is very useful and important in many applications that include analgesic and antipyretic drugs, photographic developer, corrosion inhibitor, anticorrosion lubricant, etc. [17,37]. The AuNPs/TWEEN/GO composites were used in the catalytic reduction of 4-NP by sodium borohydride in the presence of noble metal nanoparticles as catalysts has been intensively investigated for the efficient production of 4-AP [38,39]. The pure 4-NP shows a distinct spectral profile with an absorption maximum at 316 nm, as shown in Fig. 7A. It is clearly seen that a new absorption peak was observed at 400 nm when $NaBH_4$ solution was added into the 4-NP in the presence of AuNPs/TWEEN/GO composites, as shown in Fig. 7B. The absorption intensity of 4-NP at 400 nm

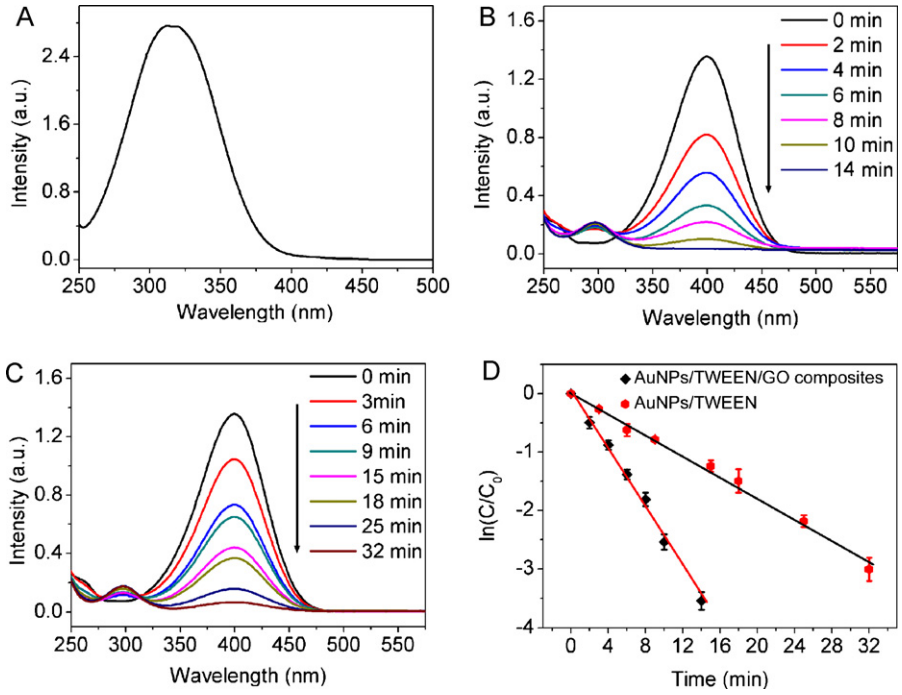

Fig. 7. (A) UV–vis absorption spectra of 4-NP and time dependent absorption spectra for the catalytic reduction of 4-NP by $NaBH_4$ in the presence of (B) AuNPs/TWEEN/GO composites and (C) AuNPs/TWEEN. (D) Plot of ln (C_t/C_0) of 4-NP against time for the catalysts. Conditions: [4-NP] = 3.5 mM; [Catalyst] = 2.16 mM; [$NaBH_4$] = 80 mM.

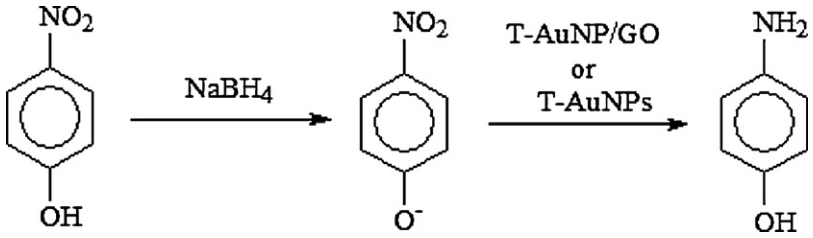

Fig. 8. The total reduction reaction for the conversion of 4-NP to 4-AP.

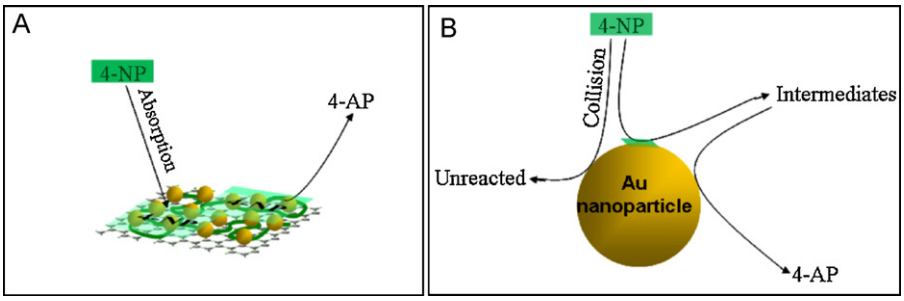

Scheme 2. A scheme (not to scale) to illustrate the proposed mechanism of the conversion of 4-NP to 4-AP by (A) AuNPs/TWEEN/GO composites and (B) AuNPs/TWEEN.

decreased quickly with elapsed time, accompanied by the appearance of the peak of 4-AP at 300 nm, indicating successful conversion of 4-NP to 4-AP. The total reduction reaction is summarized in Fig. 8. The full reduction of 4-NP by $NaBH_4$ was completed within 14 min upon the addition of 100 μL of AuNPs/TWEEN/GO composites, with the observation of a fading and ultimate bleaching of the yellow-green color of reaction mixture in aqueous solution. However, a longer reaction time of 32 min was required to achieve the full reduction of 4-NP by $NaBH_4$ using 100 μL of AuNPs/TWEEN dispersion as catalysts, as shown in Fig. 7C. Note that, without the addition of catalyst, the reduction will not proceed, and the absorption peak centered at 400 nm remains unaltered over time. Due to the presence of large excess $NaBH_4$ compared to 4-NP, the rate of reduction is independent of the concentration of $NaBH_4$, and the reaction could be considered pseudo-first-order with respect to the concentration of 4-NP [40]. Hence, ln (C_t/C_0) vs. time can be obtained based on the absorbance as the function of time, and good linear correlations are observed, as shown in Fig. 7D, suggesting that the reactions follow pseudo-first-order kinetics. Then, the kinetic reaction rate constants (defined as k_{app}) are estimated from the slopes of the linear relationship to be 25.37×10^{-2} min^{-1} and 9.05×10^{-2} min^{-1} for AuNPs/TWEEN/GO composites and AuNPs/TWEEN, respectively. These results clearly indicate the AuNPs/TWEEN/GO composites have higher catalytic activity for the reduction of 4-NP than the AuNPs/TWEEN counterparts, which can be attributed to that the GO supports play an active part in the catalysis, yielding a synergistic effect [41]. The synergistically enhanced catalytic activity may be explained as follows: it is expected that 4-NP can be adsorbed onto GO via π–π stacking interactions as 4-NP is π-rich in nature. Such adsorption provides a high concentration of 4-NP near to the AuNPs on GO, leading to highly efficient contact between them as shown in Scheme 2A. In contrast, without a highly adsorbent GO support, 4-NP must collide with AuNPs by chance, and remains in contact for the catalysis to proceed. When this is not achieved, 4-NP will pass back into solution and can only react further when it collides with AuNPs again [42], as shown in Scheme 2B. All the above observations indicate that AuNPs/TWEEN/GO composites exhibit good catalytic activity toward 4-NP reduction and the GO supports also enhance the catalytic activity via a synergistic effect.

4. Conclusions

In summary, we have developed a environment friendly route for the synthesis of AuNPs on TWEEN-functionalized GO using TWEEN 20 as a stabilizing agent for GO as well as a reducing and immobilizing agent for Au nanoparticles. These AuNPs/TWEEN/GO composites are found to exhibit remarkable catalytic performance for hydrazine oxidation. The hydrazine sensor based on AuNPs/TWEEN/GO composites has a lower detection limit, which can be used in environmental monitoring. They also exhibit good catalytic performance toward 4-NP reduction. The GO supports not only enhance the catalytic activity of AuNPs via a synergistic effect, but lend the AuNPs/TWEEN/GO composites the easiness of separation and recovery for practical catalytic applications. Such AuNPs/TWEEN/GO composites may hold great promise for applications in areas including biosensor, environmental monitoring, analytical and electroanalytical chemistry.

Acknowledgement

This work was supported by National Basic Research Program of China (No. 2011CB935800).

References

[1] X. Huang, X. Yin, S. Wu, X. Qi, Q. He, Q. Zhang, Q. Yan, F. Boey, H. Zhang, Graphene-based materials: synthesis, characterization, properties, and applications, Small 7 (2011) 1876–1902.
[2] H. Jiang, Chemical Preparation of graphene-based nanomaterials and their applications in chemical and biological sensors, Small 7 (2011) 2413–2427.
[3] X. Huang, X. Qi, F. Boey, H. Zhang, Graphene-based composites, Chem. Soc. Rev. (2011), doi:10.1039/c1cs15078b.
[4] Y. Wang, Z. Li, J. Wang, J. Li, Y. Lin, Graphene and graphene oxide: biofunctionalization and applications in biotechnology, Trends Biotechnol. 29 (2011) 205–212.
[5] S. Yang, X. Feng, L. Wang, K. Tang, J. Maier, K. Mullen, Graphene-based nanosheets with a sandwich structure, Angew. Chem. Int. Ed. 49 (2010) 4795–4799.
[6] M.L. Teague, A.P. Lai, J. Velasco, C.R. Hughes, A.D. Beyer, M.W. Bockrath, C.N. Lau, N.C. Yeh, Evidence for strain-induced local conductance modulations in single-layer graphene on SiO_2, Nano Lett. 9 (2009) 2542.
[7] X. Cao, Q. He, W. Shi, B. Li, Z. Zeng, Y. Shi, Q. Yan, H. Zhang, Graphene oxide as a carbon source for controlled growth of carbon nanowires, Small 7 (2011) 1199–1202.

[8] J.C. Meyer, A.K. Geim, M.I. Katsnelson, K.S. Novoselov, T.J. Booth, S. Roth, The structure of suspended graphene sheets, Nature 446 (2007) 60.
[9] X. Zhou, X. Huang, X. Qi, S. Wu, C. Xue, F.Y.C. Boey, Q. Yan, P. Chen, H. Zhang, In situ synthesis of metal nanoparticles on single-layer graphene oxide and reduced graphene oxide surface, J. Phys. Chem. C 113 (2009) 10842.
[10] X. Huang, S. Li, Y. Huang, S. Wu, X. Zhou, S. Li, C.L. Gan, F. Boey, C.A. Mirkin, H. Zhang, Synthesis of hexagonal close-packed gold nanostructures, Nat. Commun. 2 (2011) 292.
[11] X. Huang, X. Zhou, S. Wu, Y. Wei, X. Qi, J. Zhang, F. Boey, H. Zhang, Reduced graphene oxide-templated photochemical synthesis and in situ assembly of Au nanodots to orderly patterned Au nanodot chains, Small 6 (2010) 513–516.
[12] F. Bei, X. Hou, S.L.Y. Chang, G.P. Simon, D. Li, Interfacing colloidal graphene oxide sheets with gold nanoparticles, Chem. Eur. J. 17 (2011) 5958–5964.
[13] N. Zhang, H. Qiu, Y. Liu, W. Wang, Y. Li, X. Wang, J. Gao, Fabrication of gold nanoparticle/graphene oxide nanocomposites and their excellent catalytic performance, J. Mater. Chem. 21 (2011) 11080–11083.
[14] J. Li, X. Lin, Electrocatalytic oxidation of hydrazine and hydroxylamine at gold nanoparticle-polypyrrole nanowire modified glassy carbon electrode, Sens. Actuators B 126 (2007) 527–535.
[15] S. Guo, J. Li, W. Ren, D. Wen, S. Dong, E. Wang, Carbon nanotube/silica coaxial nanocable as a three-dimensional support for loading diverse ultra-high-density metal nanostructures: facile preparation and use as enhanced materials for electrochemical devices and SERS, Chem. Mater. 21 (2009) 2247–2257.
[16] F. Wang, X. Deng, W. Wang, Z. Chen, Nitric oxide measurement in biological and pharmaceutical samples by an electrochemical sensor, J. Solid State Electrochem. 15 (2011) 829–836.
[17] Z. Zhang, C. Shao, P, Zou, P. Zhang, M. Zhang, J. Mu, Z. Guo, X. Li, C. Wang, Y. Liu, In situ assembly of well-dispersed gold nanoparticles on electrospun silica nanotubes for catalytic reduction of 4-nitrophenol, Nanoscale 3 (2011) 3357–3363.
[18] T.A. Pham, B.C. Choi, K.T. Lim, Y.T. Jeong, A simple approach for immobilization of gold nanoparticles on graphene oxide sheets by covalent bonding, Appl. Surf. Sci. 257 (2011) 3350–3357.
[19] K. Yamada, K. Yasuda, N. Fujiwara, Z. Siroma, H. Tanaka, Y. Miyazaki, T. Kobayashi, Potential application of anion-exchange membrane for hydrazine fuel cell electrolyte, Electrochem. Commun. 5 (2003) 892–896.
[20] S.D. Zelnick, D.R. Mattile, P.C. Stepaniak, Occupational exposure to hydrazines: treatment of acute central nervous system toxicity, Aviat. Space Environ. Med. 74 (2003) 1285–1291.
[21] S. Garrod, M.E. Bollard, A.W. Nicholls, S.C. Connor, J. Connelly, J.K. Nicholson, E. Holmes, Integrated metabonomic analysis of the multiorgan effects of hydrazine toxicity in the rat, Chem. Res. Toxicol. 18 (2005) 115–122.
[22] W.X. Yin, Z.P. Li, J.K. Zhu, H.Y. Qin, Effects of NaOH addition on performance of the direct hydrazine fuel cell, J. Power Sources 182 (2008) 520–523.
[23] S.S. Narayanan, F. Scholz, A comparative study of the electrocatalytic activities of some metal hexacyanoferrates for the oxidation of hydrazine, Electroanalysis 11 (1999) 465–469.
[24] S. Panigrahi, S. Basu, S. Praharaj, S. Pande, S. Jana, A. Pal, S.K. Ghosh, T. Pal, Synthesis and size-selective catalysis by supported gold nanoparticles: study on heterogeneous and homogeneous catalytic process, J. Phys. Chem. C 111 (2007) 4596–4605.
[25] T. Vincent, E. Guibal, Chitosan-supported Palladium catalyst. 3. Influence of experimental parameters on nitrophenol degradation, Langmuir 19 (2003) 8475–8483.
[26] D. Wei, Y. Ye, X. Jia, C. Yuan, W. Qian, Chitosan as an active support for assembly of metal nanoparticles and application of the resultant bioconjugates in catalysis, Carbohydr. Res. 345 (2010) 74–81.
[27] S. Park, N. Mohanty, J.W. Suk, A. Nagarja, J. An, R.D. Piner, W. Cai, D.R. Dreyer, V. Berry, R.S. Ruoff, Biocompatible, robust free-standing paper composed of a TWEEN/graphene composite, Adv. Mater. 22 (2010) 1–5.
[28] W.S. Hummers, R.E. Offeman, Preparation of graphitic oxide, J. Am. Chem. Soc. 80 (1958), 1339-1339.
[29] J.I. Paredes, S. Villar-Rodil, A.M. Alonso, J.M.D. Tascon, Graphene oxide dispersions in organic solvents, Langmuir 24 (2008) 10560–10564.
[30] J. Li, C. Liu, Ag/graphene heterostructures: synthesis, characterization and optical properties, Eur. J. Inorg. Chem. (2010) 1244–1248.
[31] T. Szabo, O. Berkesi, P. Forgo, K. Josepovits, Y. Sanakis, D. Petridis, I. Dekany, Evolution of surface functional groups in a series of progressively oxidized graphite oxides, Chem. Mater. 18 (2006) 2740–2749.
[32] C. Xu, X. Wang, J. Zhu, X. Yang, L. Lu, Deposition of Co_3O_4 nanoparticles onto exfoliated graphite oxide sheets, J. Mater. Chem. 18 (2008) 5625–5629.
[33] S. Wang, K. Qian, X. Bi, W. Huang, Influence of speciation of aqueous $HAuCl_4$ on the synthesis, structure, and property of Au colloids, J. Phys. Chem. C 113 (2009) 6505–6510.
[34] X. Fan, L. Liu, Z. Guo, N. Gu, L. Xu, Y. Zhang, Facile synthesis of networked gold nanowires based on the redox characters of aniline, Mater. Lett. 64 (2010) 2652–2654.
[35] G. Chang, Y. Luo, W. Lu, J. Hu, F. Liao, X. Sun, Immobilization of Au nanoparticles on Au electrode for hydrazine detection: using thiolated single-stranded DNA as a linker, Thin Solid Films 519 (2011) 6130–6134.
[36] A. Umar, M.M. Rahman, S.H. Kim, Y.B. Hahn, Zinc oxide nanonail based chemical sensor for hydrazine detection, Chem. Commun. (2008) 166–168.
[37] Y. Du, H. Chen, R. Chen, N. Xu, Synthesis of *p*-aminophenol from *p*-nitrophenol over nano-sized nickel catalysts, Appl. Catal. A 277 (2004) 259–264.
[38] Y. Deng, Y. Cai, Z. Sun, J. Liu, C. Liu, J. Wei, W. Li, C. Liu, Y. Wang, D. Zhao, Multifunctional mesoporous composite microspheres with well-designed nanostructure: a highly intergrated catalyst system, J. Am. Chem. Soc. 132 (2010) 8466–8473.
[39] M. Yu, S. Geeta, L. Yan, B. Matthias, High catalytic activity of platinum nanoparticles immobilized on spherical polyelectrolyte brushes, Langmuir 21 (2005) 12229–12234.
[40] J. Huang, S. Vongehr, S. Tang, H. Lu, X. Meng, Highly catalytic Pd–Ag bimetallic dendrites, J. Phys. Chem. C 114 (2010) 15005–15010.
[41] Y. Zhang, S. Liu, W. Lu, L. Wang, J. Tian, X. Sun, In situ green synthesis of Au nanostructures on graphene oxide and their application for catalytic reduction of 4-nitrophenol, Catal. Sci. Technol. 1 (2011) 1142–1144.
[42] R. Leary, A. Westwood, Carbonaceous nanomaterials for the enhancement of TiO_2 photocatalysis, Carbon 49 (2011) 741–772.